



# A Protective Role of Tumor Necrosis Factor Superfamily-15 in Intracerebral Hemorrhage-Induced Secondary Brain Injury

ASN Neuro  
Volume 13: 1–12  
© The Author(s) 2021  
Article reuse guidelines:  
sagepub.com/journals-permissions  
DOI: 10.1177/17590914211038441  
journals.sagepub.com/home/asn  


Gui-Li Yang<sup>1,\*</sup> , Shizhao Wang<sup>2,\*</sup>, Shu Zhang<sup>1</sup>, Ye Liu<sup>1</sup>, Xiao Liu<sup>1</sup>, Dong Wang<sup>1</sup>, Huijie Wei<sup>1</sup>, Jianhua Xiong<sup>1</sup>, Zhi-Song Zhang<sup>3</sup>, Zengguang Wang<sup>1</sup>, Lu-Yuan Li<sup>3</sup>, and Jianning Zhang<sup>1</sup>

## Abstract

Destabilization of blood vessels by the activities of vascular endothelial growth factor (VEGF) and matrix metalloproteinases (MMPs) following intracerebral hemorrhage (ICH) has been considered the main causes of aggravated secondary brain injury. Here, we show that tumor necrosis factor superfamily-15 (TNFSF15; also known as vascular endothelial growth inhibitor), an inhibitor of VEGF-induced vascular hyper-permeability, when overexpressed in transgenic mice, exhibits a neuroprotective function post-ICH. In this study, we set-up a collagenase-induced ICH model with TNFSF15-transgenic mice and their transgene-negative littermates. We observed less lesion volume and neural function perturbations, together with less severe secondary injuries in the acute phase that are associated with brain edema and inflammation, including vascular permeability, oxidative stress, microglia/macrophage activation and neutrophil infiltration, and neuron degeneration, in the TNFSF15 group compared with the littermate group. Additionally, we show that there is an inhibition of VEGF-induced elevation of MMP-9 in the perihematomal blood vessels of the TNFSF15 mice following ICH, concomitant with enhanced pericyte coverage of the perihematomal blood vessels. These findings are consistent with the view that TNFSF15 may have a potential as a therapeutic agent for the treatment of secondary injuries in the early phase of ICH.

## Keywords

tumor necrosis factor superfamily-15, intracerebral hemorrhage, matrix metalloproteinases, secondary brain injury, inflammation, blood–brain barrier

Received March 23, 2021; Revised July 16, 2021; Accepted for publication July 22, 2021

## Introduction

Intracerebral hemorrhage (ICH) is an important public health problem with high mortality and morbidity. Development of therapeutic intervention approaches has focused on the prevention of hematoma expansion and brain edema, however, efforts have not led to improved outcomes (Zhu et al., 2019). It is recognized that inflammatory cascade and increased vascular permeability after ICH attribute significantly to the formation of brain edema and perihematomal edema (PHE) expansion, which accelerate neuron cell death (Urday et al., 2015). Post-ICH inflammation involves infiltration of neutrophils and macrophages, activation of microglia and astrocytes, and consequently production of inflammatory mediators including cytokines, reactive oxygen species (ROS), and matrix metalloproteinases (MMPs) (Wang & Doré, 2007). Elevated

<sup>1</sup>Department of Neurosurgery, Tianjin Medical University General Hospital; Tianjin Neurological Institute; Key Laboratory of Post-trauma Neuro-repair and Regeneration in Central Nervous System, Ministry of Education; Tianjin Key Laboratory of Injuries, Variations and Regeneration of Nervous System, Tianjin, China

<sup>2</sup>North China University of Science and Technology Affiliated Hospital, Tangshan, HeBei Province, China

<sup>3</sup>State Key Laboratory of Medicinal Chemical Biology, Nankai University College of Pharmacy, Tianjin Key Laboratory of Molecular Drug Research, Tianjin, China

### Corresponding Authors:

Lu-Yuan Li, Nankai University, 94 Weijin Road, New Life Sciences Building A307, Tianjin 300071, China.  
Email: liluyuan@nankai.edu.cn

Jianning Zhang, Department of Neurosurgery, Tianjin Medical University General Hospital, Tianjin Neurological Institute, 154 An Shan Street, Tianjin 300052, China.

E-mail: jianningzhang@hotmail.com

\*Gui-Li Yang and Shizhao Wang contributed equally to this work.



MMP activities are particularly important with regard to impairment of the integrity of blood–brain barrier (BBB) as these activities result in disruption of the basement membrane of blood vessels and the separation of pericytes from vascular endothelial cells, leading to greatly enhanced vascular permeability (Rempe et al., 2016; Rundhaug, 2005). Among the up-regulated MMPs, MMP-9 plays a dominant role in early brain injury in ICH (Wang & Tsirka, 2005). The main sources of MMP-9 include tissues undergoing abnormal angiogenesis and vascular remodeling (Chen et al., 2013) and infiltrated neutrophils enriched in the injured tissues (Atkinson & Senior, 2003). MMP-9 has been shown to disrupt the BBB (Rempe et al., 2016), and treatment with MMP inhibitors reduced brain edema and mortality in the experimental models of ICH (Lapchak et al., 2000; Pfefferkorn & Rosenberg, 2003; Rosenberg & Navratil, 1997; Wang & Tsirka, 2005).

Tumor necrosis factor superfamily-15 (TNFSF15), also known as vascular endothelial growth inhibitor (VEGI or TL1A), is a cytokine produced predominantly by endothelial cells in the blood vessels of brain and other normal tissues (Chew et al., 2002; Yang et al., 2019; Zhai et al., 1999). TNFSF15 has been shown to inhibit endothelial cell proliferation by enforcing a growth arrest on quiescent endothelial cells while inducing apoptosis in proliferating endothelial cells (Yu et al., 2001). It has been shown in a mouse model of intracranial hemangioma that TNFSF15 treatment has an inhibitory effect on intracranial hemangioma growth, lesion-associated hemorrhage, activation of macrophage/microglia, and the infiltration of MMP-9<sup>+</sup> neutrophils into intracranial hemangioma, giving rise to elevated vascular stability (Yang et al., 2019). Similarly, TNFSF15 treatment has been shown in a mouse model of traumatic brain injury (TBI) to reduce the contusion brain tissue loss, the permeation of inflammatory cells, and the activation of microglia, as well as up-regulation of tight junction proteins in endothelial cells, with an overall effect of reduced vascular permeability in the ipsilateral hemisphere (Gao et al., 2015). Studies at the molecular level have shown that perturbation of vascular permeability in brain injury is accompanied by highly elevated vascular endothelial growth factor (VEGF) levels and consequently the activation of VEGF receptor-2 (VEGFR2) (Hansen et al., 2008; Nag et al., 1997). TNFSF15 has been shown to be able to inhibit VEGF-induced VEGFR2 activation, and thus protect vascular integrity (Yang et al., 2017).

In this study, we utilized TNFSF15-overexpressing transgenic mice to establish a model of collagenase-induced ICH to investigate whether TNFSF15 has a protective effect on early brain injury. We found that high systemic levels of TNFSF15 are correlated with lowered MMP activities, improved BBB stability, and alleviated ICH injury evident from lowered extent of inflammation and reduced degree of neuron degeneration.

## Materials and Methods

### Animal Experiments

The SPC-TNFSF15-transgenic mouse strain (C57BL/6 background) was established in the laboratory of L.-Y.L (Qin et al., 2015; Yang et al., 2017, 2019). In this study, 8-week-old female SPC-TNFSF15-transgenic mice and the transgene-negative littermates were used. All animal experiments complied with the ARRIVE guidelines. All procedures involving experimental animals were performed in accordance with protocols approved by Tianjin Medical University Care and Use Committee. Animals were grouped by five and housed in a temperature-controlled room maintained on a 12-hr light/dark cycle. Food and water were available ad libitum and nesting material was added to the cage.

### ICH Model

The animals were anesthetized with pentobarbital (40 mg/kg, intraperitoneally [i.p.]). Thereafter, mice were placed in a stereotactic frame and a 1 mm hole in diameter was drilled on the right side of the skull (3 mm lateral to midline, 0.5 mm anterior to bregma). We injected mice using an infusion pump (Kd Scientific Inc., Holliston, MA) in the right striatum with 0.0065 U/ $\mu$ l collagenase VII (Sigma, St. Louis, MO) in 0.5  $\mu$ l saline at a depth of 4 mm beneath the skull. Collagenase was delivered over 5 min. The needle stayed in place for an additional 5 min to prevent reflux. The overall mortality rate was <2%. During surgery, body temperature was maintained at 37 °C. The skull hole was closed with bone wax and the incision was closed with sutures following surgery. To avoid dehydration, 0.5 ml of saline (0.9% sodium chloride [NaCl]) was given to each mouse by subcutaneous injection immediately after surgery, before being placed in a cage with free access to food and water.

### Neurological Deficit

Neurological tests were conducted and scored blindly at 24, 48, or 72 hr after ICH by at least two investigators. The modified neurological severity score (mNSS) were carried out. The mNSS rates neurological functioning on a scale of 15 and includes a composite of motor, sensory, reflex, and balance tests. The mouse was given one point for the inability to perform each test while one point was deducted for the lack of a tested reflex. Finally, an overall score was given to determine impairment in each mouse. The corner turning test was used to assess sensorimotor and postural asymmetries, the tested mouse was allowed to go into a corner with an angle of 30° and was required to turn either to the left or to the right to exit the corner. This was repeated and recorded 10 times, with at least 30 s between trials, and the percentage of right turns among total turns was calculated in this study.

### **Brain Water Content Assessment**

For brain water content assessment, after euthanasia and decapitation at day 3 after ICH, brains were placed in a brain-cutting matrix. Brains were immediately divided into three parts: left hemisphere, right hemisphere, and cerebellum. The tissues were then weighed to obtain the wet weight, followed by drying for 24 hr at 100 °C to obtain the dry weight. Brain water content was calculated using the following formula:  $(\text{Wet Weight} - \text{Dry Weight}) / \text{Wet Weight} \times 100\%$ .

### **Hemorrhagic Injury Analysis**

After neurological scoring, mice were sacrificed, and their brains were removed and frozen immediately on dry ice for 5 min. Injury volumes were digitally quantified, employing ImageJ v.1.63 software, on 50  $\mu\text{m}$  coronal sections using a previously reported method of Luxol fast blue/cresyl violet staining (Wang et al., 2003). Hemorrhagic injury lesion volume was calculated by multiplying the vascular lesion areas by the thickness of the sections. Nine mice per group were analyzed by an observer blinded to the experimental treatment.

### **In Situ Detection of ROS Production**

Detection of ROS was conducted according to a previously reported method (Wang & Tsirka, 2005). At 3 days after ICH, mice were injected i.p. with 300  $\mu\text{l}$  of hydroethidine (Molecular Probes). Brains were harvested 2 hr later and frozen immediately on dry ice for 5 min, then sectioned at 30  $\mu\text{m}$ . The brain sections were coverslipped using a mounting medium with 4,6-diamidino-2-phenylindole (DAPI; Vector Labs). Ethidium was visualized on an Olympus Fluo-view 1000 confocal microscope (Olympus, Tokyo, Japan) and photographed using a digital camera system and double exposure to produce images of ethidium and DAPI. Ethidium, indicative of the presence of ROS, was quantified: Cells with ethidium extending to the cytosol were counted under high magnification in eight different sites randomly selected in at least three sections per animal and averaged in the entire field. The percentage of these cells in relation to the total cells stained with DAPI nuclear staining was then analyzed.

### **Fluoro-Jade B (FJB) Staining**

FJB staining was carried out according to published protocols (Schmued & Hopkins, 2000). Cells permeable to FJB were marked for cell death. FJB can sensitively and selectively detect degenerating neurons. Degenerating neurons adjacent to the hematoma were counted in at least eight fields using a magnification of 200 $\times$  in at least three sections per animal; areas with large blood vessels were avoided. Seven

mice per group were analyzed by an observer blinded to the experimental treatment.

### **In Vivo Vascular Permeability Assay**

SPC-TNFSF15-transgenic mice and their littermates subjected to collagenase-induced ICH for 3 days received 100  $\mu\text{l}$  of 1% Evans blue (E2129, Sigma Aldrich, St. Louis, MO) through the tail vein. They were sacrificed 2 hr after injection and perfused with phosphate-buffered saline (PBS). The brains were dissected and placed in formamide (300  $\mu\text{l}$ , 56 °C, 36 hr) to extract Evans blue. The absorbance of the extraction solutions was measured at 620 nm in a SpectraMax M5 plate-reader (Molecular Devices, Sunnyvale, CA).

### **Immunofluorescence**

Frozen sections were fixed with 4% paraformaldehyde for 10 min and then incubated in 10% normal donkey serum for 1 hr before they were incubated with the following antibodies at 4 °C overnight: anti-CD68 (1:100, Bio-Rad, cat. no. MCA1957, RRID: AB\_322219), anti-neutrophil Ly6B.2 (clone 7/4) (1:100, Bio-Rad, cat. no. MCA771GA, RRID: AB\_324243), anti-matrix metalloproteinase 9 (MMP-9) (5  $\mu\text{g}/\text{ml}$ , R&D Systems, cat. no. AF909, RRID: AB\_355706), anti-CD31 (10  $\mu\text{g}/\text{ml}$ , R&D Systems, cat. no. AF3628, RRID: AB\_2161028), anti-claudin-5 (1:200, Abcam, cat. no. ab15106, RRID: AB\_301652), anti-CD31 (1:50, Santa Cruz Biotechnology, cat. no. sc-28188, RRID: AB\_2267979), and anti-Desmin (1:200, Santa Cruz Biotechnology, cat. no. sc-14026, RRID: AB\_2092608). The sections were incubated for 90 min with the corresponding secondary antibodies (1:250, Thermo Fisher Scientific, cat. no. A-21208, RRID: AB\_2535794; Thermo Fisher Scientific, cat. no. A-21432, RRID: AB\_2535853; Thermo Fisher Scientific, cat. no. A-21206, RRID: AB\_2535792; Thermo Fisher Scientific, cat. no. A-21209, RRID: AB\_2535795; Thermo Fisher Scientific, cat. no. A-11055, RRID: AB\_2534102). The slides were mounted and subjected to microscopic analysis with a Nikon NIS-Elements microscope (Nikon, Tokyo, Japan) or an Olympus Fluo-view 1000 confocal microscope (Olympus, Tokyo, Japan). A total of six images were randomly taken in the area adjacent to hematoma of each section. Six mice per group were analyzed by an observer blind to the experimental treatment.

### **In Situ Zymography and Double Labeling With Fluorescent Probes**

In situ gelatinolytic activity was detected on frozen brain sections of 10  $\mu\text{m}$  thick using a commercial kit (EnzChek Gelatinase Assay kit; Molecular Probes, Eugene, OR). Fresh sections were incubated with DQ gelatin conjugate,

a fluorogenic substrate, at 37 °C for 1 hr and washed and fixed in 4% paraformaldehyde in PBS. Cleavage of DQ gelatin by MMPs results in a green fluorescent product (excitation, 495 nm; emission, 515 nm). Gelatinolytic activity-positive cells were counted in six fields immediately adjacent to the hematoma; large blood vessels were avoided.

### Gelatinase/Collagenase Activity Assay

To analyze collagenase activity, the Enzchek Gelatinase/Collagenase Assay Kit (Invitrogen) was used according to manufacturer's instructions. Ipsilateral brain tissues were obtained after 3 days of ICH. The tissues were homogenated with a motor-driven Teflon pestle for 5 min on ice in 500  $\mu$ l extraction buffer (25 mM Tris, pH 7.4, 100 mM NaCl, 20 mM  $\text{NH}_4\text{HCO}_3$ ) per 50 mg tissue wet weight, and the tissue extract obtained after centrifugation at 15,000g for 20 min at 4 °C was used for the gelatinase/collagenase activity assay. A brain tissue extract of 50  $\mu$ g in 80  $\mu$ l 1 $\times$  reaction buffer will be used for each 200  $\mu$ l reaction. DQ collagen fluorescein conjugate was added to each assay well. This was incubated for 24 hr at room temperature, protected from

light, and fluorescence was measured at 1, 6, 12, and 24 hr. The fluorescence was measured at 485 nm.

### Statistics

All data are presented as mean  $\pm$  SD. Prism 7 (GraphPad Software, La Jolla, CA, USA) was used for statistical analyses. Two-tailed unpaired Student's *t*-test was used to determine the significance of two groups. One-way analysis of variance (ANOVA) or two-way ANOVA was used for multiple group comparisons. Statistical significance was set at  $p < .05$ .

### Results

#### Collagenase-Induced ICH is Less Severe in TNFSF15-Overexpressing Transgenic Mice

To determine the impact of TNFSF15 on early brain injury in ICH, we set-up an ICH model by intracranial injection of collagenase into the ipsilateral hemispheres of TNFSF15-overexpressing transgenic mice (SPC-TNFSF15) (Yang et al., 2019) and their transgene-negative littermates. We measured the ICH lesion volume with Luxol fast blue/cresyl violet staining on day 3 postinjury, and found that the lesion volumes in the TNFSF15 group were about 50% of those in the littermates (Figure 1A and B). We evaluated ICH-associated neurodeficits by carrying out an mNSS test and corner turning test at days 1, 2, and 3 postinjury. The mNSS scores and corner turning test were consistently improved in the transgenic group compared with those in the littermates during the entire duration of the experiment (Figure 1C and D). These results are consistent with the view that TNFSF15 may have exerted a stabilizing effect on the integrity of the brain vasculature such that the collagen-induced ICH is less severe and consequently the damages to the neural functions are more moderate.

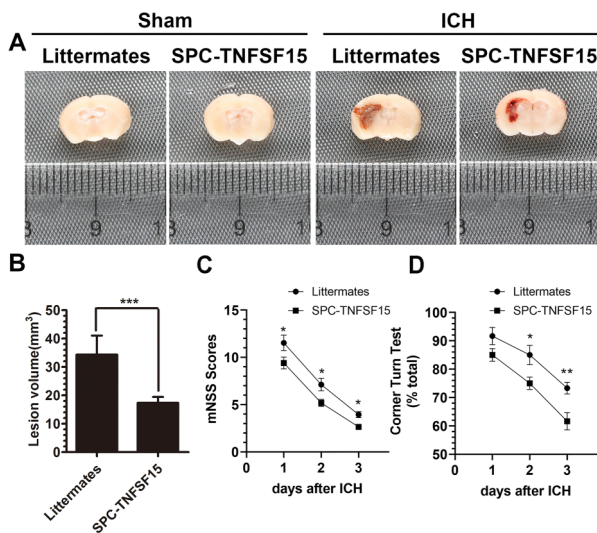


**Figure 1.** TNFSF15 attenuates lesion volume and neurodeficits in collagenase-induced ICH mouse model. (A) The representative images show that the degree of ICH in the sham group, littermates, and SPC-TNFSF15 group after collagenase injection for 3 days. (B) The quantitative analysis shows the lesion volume of collagenase-induced ICH in littermates and SPC-TNFSF15 group at day 3, unpaired *t*-test,  $n = 9$  per group. (C and D) The before–after graph showing the mNSS scores ( $n = 17$  per group) and corner turning test ( $n = 10$  per group) results of littermates and SPC-TNFSF15-transgenic mice at days 1, 2, and 3 postinjury, two-way ANOVA. The values in the bar graphs are mean  $\pm$  SD. \* $p < .05$ , \*\* $p < .01$ , \*\*\* $p < .001$ .

Note. TNFSF15 = tumor necrosis factor superfamily-15; ICH = intracerebral hemorrhage; mNSS = modified neurological severity score; ANOVA = analysis of variance; SD = standard deviation.

#### TNFSF15 Reduces ROS Production and the Number of Degrading Neurons After ICH

Because ROS production after ICH can cause neuron damage (Duan et al., 2016), we determined intracranial ROS levels postcollagenase-induced injury. We injected hydroethidine, a redox-sensitive probe that can be oxidized to ethidium by superoxide, on day 3 systemically (i.p.) into the experimental animals. We analyzed the ethidium signal in the brain section by immunostaining, and found that the number of red fluorescent ethidium-positive cells around the ICH lesions in SPC-TNFSF15 group was 41% lower than that in the littermate control group (Figure 2A and B). Additionally, we determined neuron cell death in the lesions on day 3 by using FJB staining, and found that the mean number of degenerating neurons (FJB-positive, green fluorescence; Figure 2C) in

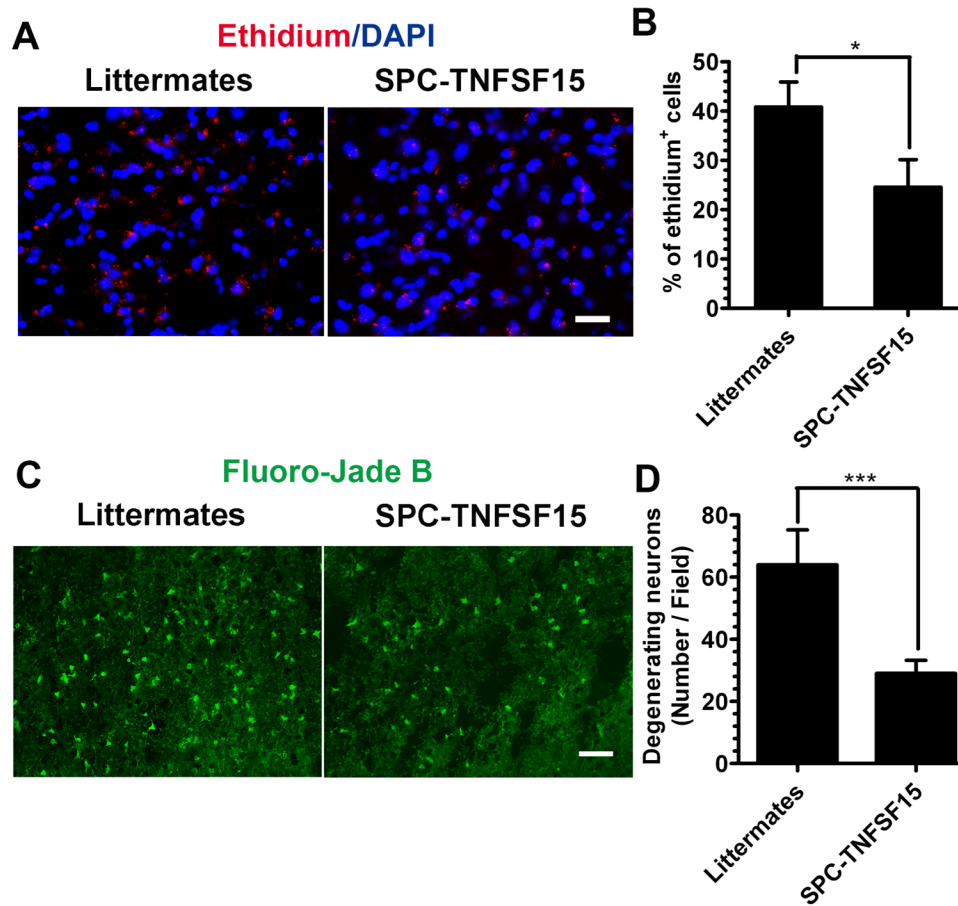


**Figure 2.** TNFSF15 decreased the production of ROS and degenerating neurons after ICH. (A) After 3 days of ICH, the peri-ICH region showed significantly increased ethidium signals (red) in the littermate group. In the SPC-TNFSF15-transgenic mice, fewer ethidium signals were detected (red). Scale bar, 50  $\mu$ m. (B) The quantitative analysis shows the number of ethidium positive cells in littermates and SPC-TNFSF15 group at day 3 after ICH, unpaired *t*-test, *n* = 7 per group. (C) Increased FJB staining were detected in the littermate group (green) compared with those in the SPC-TNFSF15 group. Scale bar, 50  $\mu$ m (D) The quantitative analysis shows the number of degenerating neurons in littermates and SPC-TNFSF15 group at 3 days, unpaired *t*-test, *n* = 7 per group. The values in the bar graphs are mean  $\pm$  SD. \**p* < .05, \*\*\**p* < .001.

Note. TNFSF15 = tumor necrosis factor superfamily-15; ROS = reactive oxygen species; ICH = intracerebral hemorrhage; FJB = fluoro-jade B.

SPC-TNFSF15-transgenic mice was about 56% of that in the littermates (Figure 2D). These results suggest that high TNFSF15 levels in the body may have prevented neuronal death caused by an increased ROS production in ICH.

### TNFSF15 Inhibits the Infiltration of Leukocytes After ICH

As excessive inflammation response aggravates brain injury in ICH, we determined the impact of TNFSF15 on activation and infiltration of leukocytes in the early phase of ICH by quantitatively analyzing the two main leukocytes, macrophage/microglia (MM) and neutrophils, in the outskirts of the ICH lesions on day 3. Immunostaining of the brain sections revealed that there was a significant activation and infiltration of CD68<sup>+</sup> macrophage/microglia in the TNFSF15

transgene-negative littermates; however, macrophage/microglia infiltration was about 40% lower in the TNFSF15-transgenic mice (Figure 3A and B). We also analyzed the infiltration of neutrophils on day 3, and found that the infiltration of Ly-6B.2-marked neutrophils in the SPC-TNFSF15 group was 33% of that in the littermates (Figure 3C and D). These results indicate that TNFSF15 may have an inhibitory effect on the marked inflammation response associated with ICH.

### TNFSF15 Attenuates Brain Edema and BBB Permeability

We determined how TNFSF15 affects brain edema following ICH by measuring the brain water content, using the wet/dry weight method. We found that the brain water content in

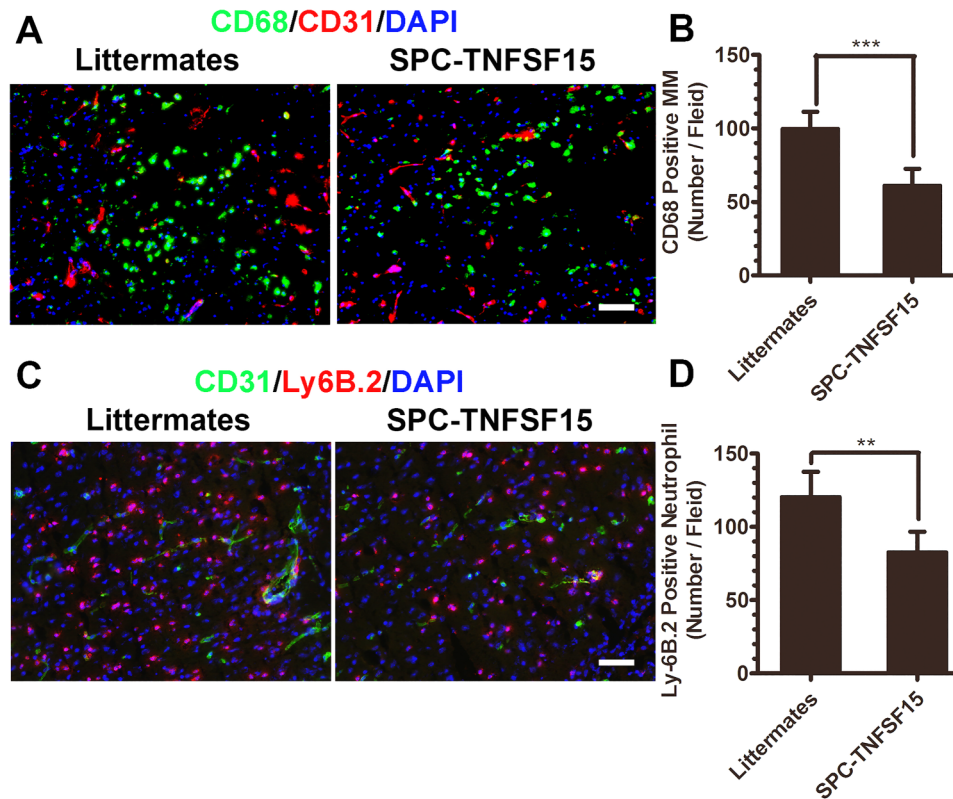


**Figure 3.** TNFSF15 decreased leukocyte recruitment after 3 days of ICH. (A) Infiltrated macrophages are present near the hematoma. Representative images showing the cellular location of CD68-positive cells with respect to the CD31-marked vessels in littermates and SPC-TNFSF15-transgenic mice. Macrophage infiltration was inhibited in SPC-TNFSF15-transgenic mice on day 3 after ICH. Scale bar, 50  $\mu$ m. (B) The numbers of macrophages were quantified in the peri-ICH region on day 3 after ICH, unpaired *t*-test,  $n = 7$  per group. (C) Infiltrated neutrophils are present near the hematoma on day 3. Representative images showing the cellular location of Ly6B.2-positive cells with respect to the CD31-marked vessels in littermates and SPC-TNFSF15-transgenic mice. Neutrophil infiltration was inhibited in SPC-TNFSF15-transgenic mice on day 3 after ICH. Scale bar, 50  $\mu$ m. (D) The numbers of neutrophils were quantified in the peri-ICH region on day 3, unpaired *t*-test,  $n = 7$  per group. The values in the bar graphs are mean  $\pm$  SD. \*\* $p < .01$ , \*\*\* $p < .001$ .  
*Note.* TNFSF15 = tumor necrosis factor superfamily-15; ICH = intracerebral hemorrhage.

SPC-TNFSF15-transgenic mice ( $78.5 \pm 0.24\%$ ) was substantially lower than that in the littermates ( $80.1 \pm 0.89\%$ ), and was very close to that in the sham group ( $77.85 \pm 0.47\%$ ) (Figure 4A). We then examined the integrity of the BBB in these experimental animals by monitoring Evans blue leakage into the brains. Evans blue dye was given to the animals by tail vein injection 2 hr prior to sample collection. The blue dye was extracted with formamide for 36 hr. Extraction of formamide resulted in the whole brains being transparent and the lesions optical (Figure 4B), revealing substantially smaller ICH lesion volume in the SPC-TNFSF15 mice compared with those in the littermates. Colorimetric analysis of the extractions indicated that dye leakage in the brains of the SPC-TNFSF15 group was about 45% lower than that in the littermate group (Figure 4C). To further investigate the impact of TNFSF15 on tight junction protein following ICH, we quantified the expression of claudin-5 using immunofluorescence staining at 3 days after ICH. Immunostaining shows that TNFSF15 preserved claudin-5

after ICH (Figure 4D). The ratio of claudin-5 expression to CD31 expression in the perihematomal blood vessels in the SPC-TNFSF15 group is approximately 2 times than that in the littermate group (Figure 4E). However, the claudin-5-to-CD31 fluorescent density ratio was consistent in their sham group (Fig. S1). These findings are consistent with the view that the ability of TNFSF15 to maintain the integrity of BBB may have attributed to ICH-induced brain edema.

#### Decreased Serum VEGF Levels and ICH Lesion Gelatinase/Collagenase Activities in TNFSF15-Transgenic Mice

We determined the blood levels of VEGF and TNFSF15 proteins by an enzyme-linked immunosorbent assay (ELISA) in the experimental animals on day 3 post-ICH. The TNFSF15 protein levels in the transgenic group were about 2 times than those in the littermate group (Figure 5A), whereas the

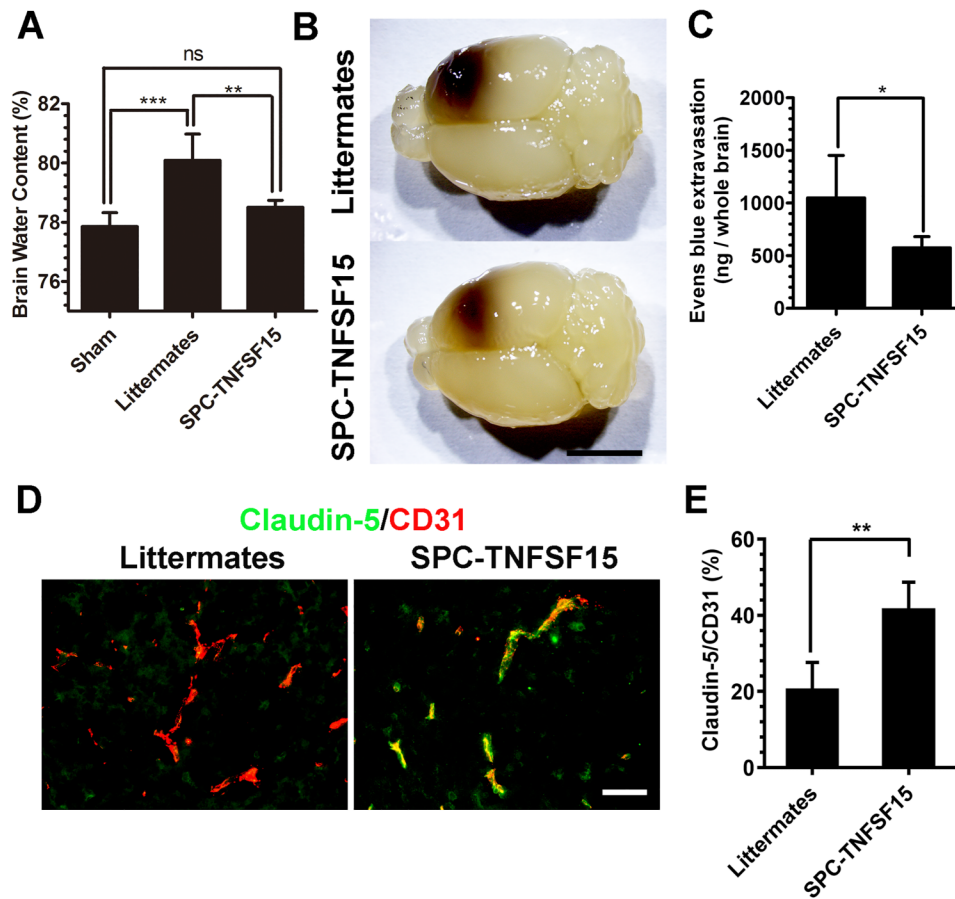


**Figure 4.** TNFSF15 suppresses brain edema and vascular permeability. (A) On day 3 after ICH, brain water content decreases in the ipsilateral hemisphere of the SPC-TNFSF15 group compared with their littermates. ANOVA,  $n=7$  per group. (B) After Evans blue extraction, the brains were transparentized. The representative images show the transparentized whole brain of littermates and SPC-TNFSF15-transgenic mice with different hematoma. (C) On day 3 after ICH, Evans blue (1%, 100  $\mu$ l) was given by tail vein injection. The whole brain undergoing Evans blue extraction in formamide for 36 hr at 56 °C. Quantification of the dye extracted from the whole brain retrieved from littermates and SPC-TNFSF15-transgenic mice after ICH at day 3, unpaired  $t$ -test,  $n=7$  per group. (D) Representative images of CD31 (red)- and claudin-5 (green)-stained sections. Scale bar, 50  $\mu$ m. (E) Bar graphs showing the claudin-5 to CD31 fluorescent density ratio in SPC-TNFSF15-transgenic mice and their littermate control group, unpaired  $t$ -test,  $n=5$  per group. The values in the bar graphs are mean  $\pm$  SD. \* $p < .05$ , \*\* $p < .01$ , \*\*\* $p < .001$ .

Note. TNFSF15 = tumor necrosis factor superfamily-15; ICH = intracerebral hemorrhage; ANOVA = analysis of variance.

VEGF protein levels were about 50% higher post-ICH in the littermate group compared with those in the SPC-TNFSF15 groups (Figure 5B). Because it was shown previously that higher levels of VEGF was correlated with an increase of MMP activities in the acute phase of stroke (Valable et al., 2005), we determined whether TNFSF15 had an impact on MMP activities in the ICH model by using in situ gelatin zymography on tissue sections. Increased MMP activities were observed in cells mostly in the peri-ICH area at 72 hr post-ICH; preincubation of the tissue sections with the MMP inhibitor 1,10-phenanthroline for 15 min resulted in the diminished MMP activities (Figure 5C). We found that the gelatinolytic activity in the SPC-TNFSF15 group was about 70% of that in their littermates (Figure 5D). Additionally, we determined gelatinase/collagenase activity

in tissue homogenates of ipsilateral hemispheres of the experimental animals, and found that these proteinase activities in the ICH lesion of the SPC-TNFSF15-transgenic mice were about 50% lower than those of the littermate controls in the first 24 hr post-ICH (Figure 5E). These results indicate that TNFSF15 inhibition of VEGF activities leads to diminishing gelatinase/collagenase activities in the ICH lesions.

#### *Diminished ICH-Induced MMP-9 Activity Associated With Perihematomal Blood Vessels in TNFSF15-Transgenic Mice*

We analyzed the vascular density of the perihematomal area in the SPC-TNFSF15 mice and littermate controls by fluorescent immunostaining for the endothelial marker CD31, and

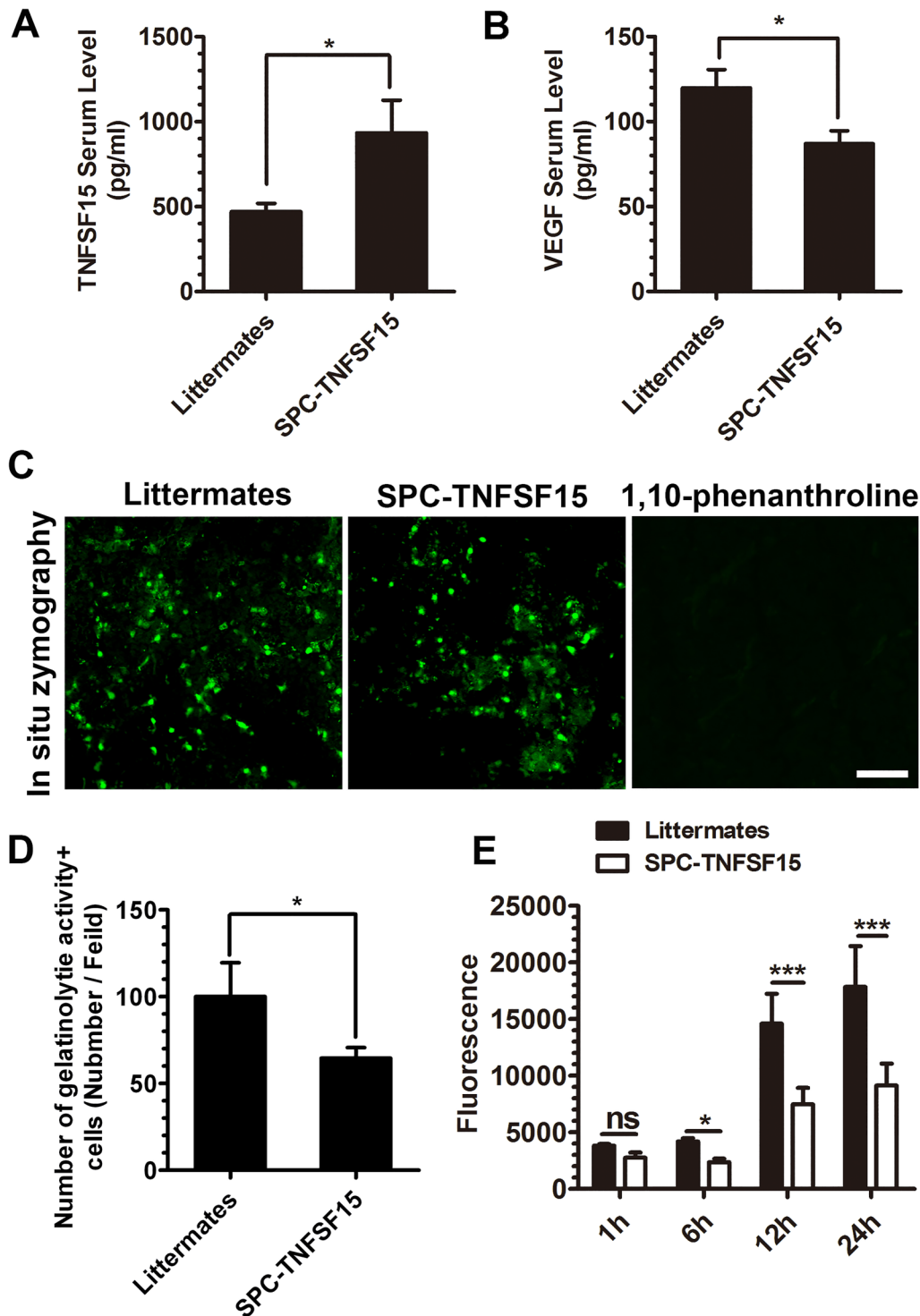


**Figure 5.** TNFSF15 decreases VEGF levels and gelatinolytic activity after ICH. (A and B) Serum levels of TNFSF15 (A) and VEGF (B) in SPC-TNFSF15-transgenic mice and transgene-negative littermates determined by ELISA, unpaired *t*-test,  $n = 7$  per group. (C) Gelatinolytic activity (green) developed after incubation of sections (20  $\mu$ m thick) with the substrate DQ gelatin or DQ gelatin and 1,10-phenanthroline. Gelatinolytic activity-positive cells are detected in the peri-injury area after ICH at 72 hr. Scale bar, 50  $\mu$ m. Decreased gelatinolytic activity was detected at 72 hr in the SPC-TNFSF15-transgenic mice group. (D) Quantification of gelatinolytic activity-positive cells after ICH, unpaired *t*-test,  $n = 7$  per group. (E) Quantification of gelatinolytic activity of brain tissue after ICH at 72 hr in vitro. The gelatinolytic activity of brain tissue was analyzed at 1, 6, 12, and 24 hr in vitro, ANOVA,  $n = 5$  per group. The values in the bar graphs are mean  $\pm$  SD. \* $p < .05$ , \*\*\* $p < .001$ .

Note. TNFSF15 = tumor necrosis factor superfamily-15; VEGF = vascular endothelial growth factor; ICH = intracerebral hemorrhage; ELISA = enzyme-linked immunosorbent assay; ANOVA = analysis of variance.



found that the vascular density of the perihematomal area in the littermate control group was 1.6 times than that in the SPC-TNFSF15 group (Figure 6A). We then determined the expression levels and locations of MMP-9 in and around the ICH lesions. Immunostaining revealed that MMP-9 positivity coincides with CD31<sup>+</sup> endothelial cells of the perihematomal blood vessels, as well as other cells in close proximity to the blood vessels (Figure 6B). We found that the number of MMP-9-associated blood vessels containing either endothelial cells or other cells adhering to blood vessels in TNFSF15-transgenic mice was 35% of that in their littermates (Figure 6C). Additionally, MMP-9 and Ly-6B.2 coimmunostaining of the perihematomal blood vessels indicate that most of the MMP-9-positive, non-endothelial cells were Ly-6B.2-positive neutrophils (Figure 6D). Moreover, because diminished MMP-9 activities on blood vessels should be accompanied by improved vascular integrity characterized by pericyte coverage of the blood vessels (Rempe et al., 2016; Rundhaug, 2005), we determined the ratio of desmin<sup>+</sup>-pericytes/smooth muscle cells to CD31<sup>+</sup>-endothelial cells in the ICH lesions in the experimental animals by immunostaining (Figure 6E), and found that the desmin-to-CD31 fluorescent density ratio in the SPC-TNFSF15 group was about 2 times that of the littermate group (Figure 6F). However, the vascular density and desmin-to-CD31 fluorescent density ratio was consistent in SPC-TNFSF15-transgenic mice and their littermates without undergoing collagenase injection (Figure S2). These data suggest that an inhibitory effect TNFSF15 exerts on MMP-9 leads to stabilization of the blood vessels in the ICH lesions.

## Discussion

The ability of TNFSF15 to inhibit the activity of VEGF/VEGFR2 to induce vascular hyperpermeability (Yang et al., 2017) appears to have a wide perspective in clinical applications concerning brain hemorrhagic diseases, as we have shown previously with experimental models of brain hemangioblastoma and TBI, which are characteristic of severe vascular leakages. In this study, we demonstrate with a mouse model of collagenase-induced ICH that systemically increased levels of TNFSF15, as in TNFSF15-overexpressing transgenic mice, are associated with markedly reduced hemorrhage volume following ICH. This is concomitant with decreased ROS, lowered MMP activities, and diminished infiltration of inflammatory cells in the ICH lesions. We further show that the blood vessels of the brain in TNFSF15-transgenic mice exhibit improved vascular wall integrity evident from decreased MMP-9 levels on the endothelial cells in the blood vessels in or around the area of PHE. Overall, neurological functions of the TNFSF15-overexpressing transgenic mice are significantly less disturbed compared with those of the transgene-negative littermates post-ICH.

It is plausible that TNFSF15 actions contribute to the reduction of the extent of inflammation in the acute phase of ICH. Decreased leukocyte recruitment after TNFSF15 treatment has been observed in three different brain disease models, including collagenase-induced ICH, intracranial hemangioma (Yang et al., 2019), and TBI (Gao et al., 2015). VEGF is known to induce macrophage/microglia activation and migration to an inflammation site via VEGFR1 on macrophage/microglia (Kerber et al., 2008) and to recruit MMP-9 expressing neutrophils (Christoffersson et al., 2012). TNFSF15 not only downregulates serum VEGF levels, but also down-modulate VEGFR1 expression (Qi et al., 2013). Thus, TNFSF15 inhibition of the VEGF/VEGFR signaling pathway may play a major role in the attenuation of inflammation after ICH. Notably, ROS are important inflammation mediators in ICH released by injured tissues to trigger activation of the immune response. Declined ROS levels in TNFSF15-transgenic mice following ICH are expected to be attributable to decreased leukocyte recruitment.

Considering ICH-induced MMP activities are suppressed in TNFSF15-transgenic mice is of importance to the stabilization of the vasculature in wounds. In response to tissue injury endothelial cells are activated to produce MMPs which leads to the degradation of vascular basement membrane, contributing to destabilization of the blood vessel wall. MMPs also stimulate VEGFR signals toward vascular remodeling (Chen et al., 2013). A number of MMP inhibitors are known to not only inhibit angiogenesis, but also block VEGFR activation (Lee et al., 2010; Seo et al., 2003). Downregulation of MMP activities in TNFSF15-transgenic mice may have resulted from the ability of TNFSF15 to inhibit the VEGF/VEGFR1 (Qi et al., 2013) and VEGF/VEGFR2 (Yang et al., 2017). Additionally, neutrophils are considered to be the major cell source of MMP-9 (Wang et al., 2019). Diminished infiltration of neutrophils in TNFSF15-transgenic mice may have led to decline an important cellular source of MMP-9 in the ICH lesions, alleviating MMP-9-facilitated vascular injury. Furthermore, MMP activities contribute to separation of pericytes from endothelial cells in blood vessels undergoing angiogenesis (Rempe et al., 2016; Rundhaug, 2005), causing lowered pericyte coverage of blood vessels. Our findings that pericyte coverage of blood vessels is elevated in ICH lesions in TNFSF15-transgenic mice suggest that TNFSF15 inhibition of angiogenesis, including inhibition of MMP activities, is beneficial to prevention of secondary brain injury in the initial phase of ICH.

In this study, we used only young female mice. This may lead to an underestimate of gender and age issues in translational settings. For instance, sex differences were known in ICH patients (Gokhale et al., 2015; Marini et al., 2017). Additionally, in terms of the ICH animal model used here, collagenase-induced ICH may have resulted in greater neurological deficit in male mice compared with female mice

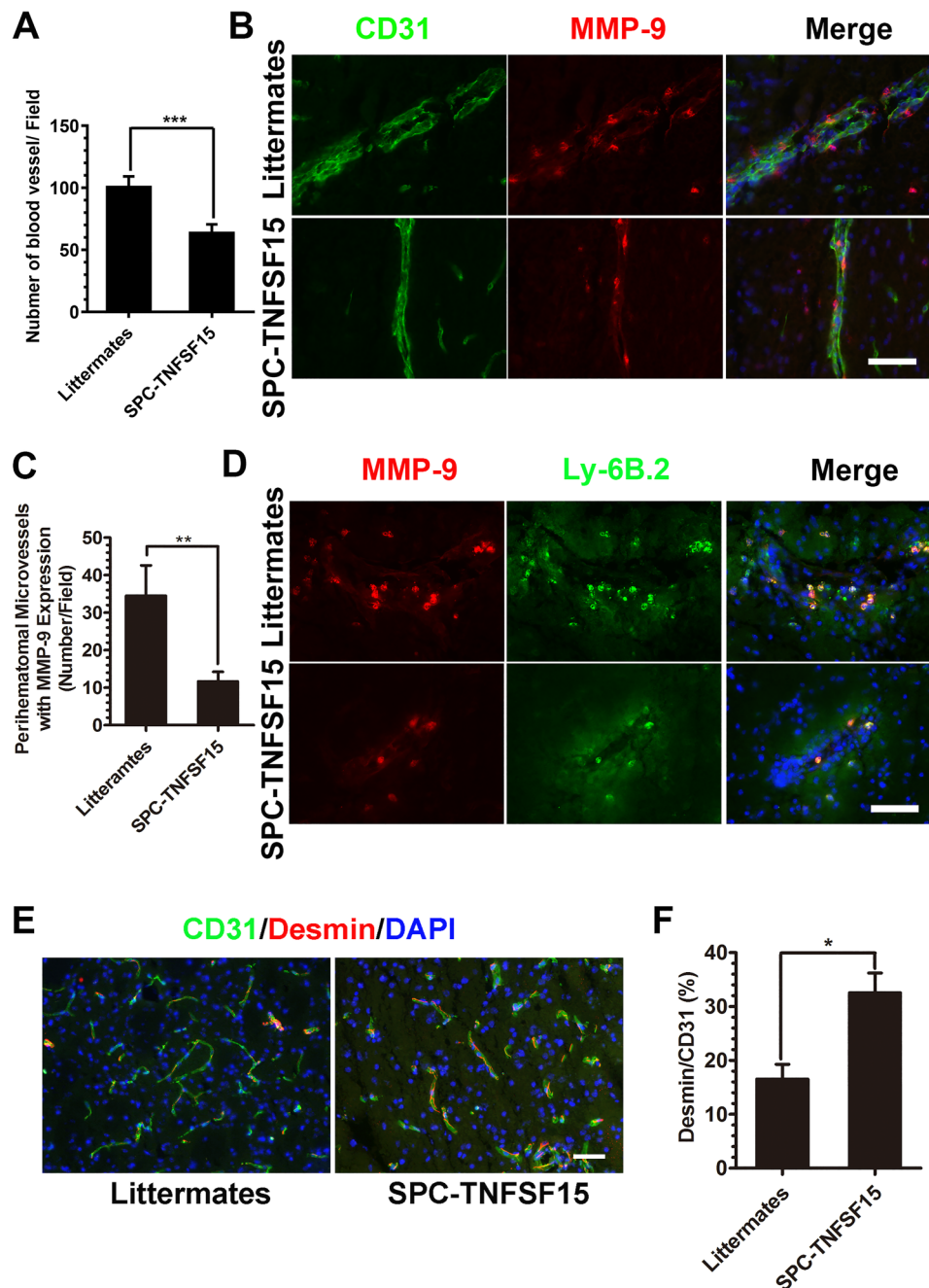


**Figure 6.** Effect of TNFSF15 and TNFSF15-induced MMP-9 change on perihematoma blood vessels after ICH. (A) Bar graphs depicting CD31-positive blood vessel densities in perihematoma blood vessels areas, unpaired *t*-test,  $n = 7$  per group. (B) Representative images showing MMP-9-positive cells in CD31-marked endothelial cells in littermates and SPC-TNFSF15-transgenic mice. Scale bar, 50  $\mu\text{m}$ . (C) Quantitative analysis of the average number of CD31-marked blood vessels with MMP-9 expression and MMP-9<sup>+</sup> cell adhesion in perihematoma blood vessels areas, unpaired *t*-test,  $n = 7$  per group. (D) Immunostaining for Ly-6B.2 (green) and MMP-9 (red) showing that MMP-9 expressing cells are neutrophils adhering to perihematoma blood vessels. Scale bar, 50  $\mu\text{m}$ . (E) Representative images of CD31 (green)- and Desmin (red)-stained sections. Scale bar, 50  $\mu\text{m}$ . (F) Bar graphs showing percentages of pericyte and smooth muscle cell coverage in the CD31<sup>+</sup> blood vessels in SPC-TNFSF15-transgenic mice and their littermate control group, unpaired *t*-test,  $n = 7$  per group. The values in the bar graphs are mean  $\pm$  SD. \* $p < .05$ , \*\* $p < .01$ , \*\*\* $p < .001$ . Note. TNFSF15 = tumor necrosis factor superfamily-15; MMP = matrix metalloproteinase-9; ICH = intracerebral hemorrhage; SD = standard deviation.

(Gokhale et al., 2015). We may have, therefore, missed responses to TNFSF15 potentially unique in male mice in collagenase-induced ICH. Moreover, the role of the estrous cycle in TNFSF15 treatment after ICH should also be considered in future studies.

In summary, our findings from this study are consistent with the view that increasing TNFSF15 levels in the acute phase of brain hemorrhage results in stabilization of blood vessels and attenuation of inflammation in wounds. The protective effect is attributable to the antiangiogenic and anti-permeability activities of TNFSF15, as these activities may have plausibly satisfied the critical need to limit secondary brain injury immediately following ICH. A balance of proangiogenic and antiangiogenic factors is then in order in the wound repair phase once ICH-associated secondary brain injury is stabilized. The time window of TNFSF15 treatment is subject to future investigations in which the dosages and timing of TNFSF15 administration are controlled.

### Author Contributions

G.-L.Y., S.Z.W., S.Z., Y.L., X.L., D.W., H.J.W., and J.H.X. performed the experiments. G.-L.Y. and S.Z.W. produced the figures. G.-L.Y., S.Z.W., Z.S.Z., Z.G.W., J.N.Z., and L.-Y.L. designed the study. G.-L.Y. and S.Z.W. analyzed the data. G.-L.Y., J.N.Z., and L.-Y.L. wrote the manuscript.

### Declaration of Conflicting Interests

The authors declared no potential conflicts of interest with respect to the research, authorship, and/or publication of this article.

### Funding

The authors disclosed receipt of the following financial support for the research, authorship, and/or publication of this article: Funding for this study was provided by the grants from the National Natural Science Foundation of China (82073064 and 81874167 to L.-Y.L., 81930031 to J.N.Z., 82071389 to G.-L.Y., 81601039 to Y.L., 81901525 to S.Z., and 81972687 to Z.S.Z.), grants from the Natural Science Foundation of Tianjin (20JCQNJC00460 to G.-L.Y. and 20JCYBJC00430 to H.J.W.), grants from the Beijing Tianjin Hebei Basic Research Cooperation Project (19JCZDJC64600(Z) to D.W.), grants from the Scientific Research Program Project of Tianjin Education Commission (2018ZD03 to Z.G.W.), and Tianjin Key Research and Development Plan, Key Project of Science and Technology Support (20YFZCSY00010 to Z.G.W.).

### ORCID iD

Gui-Li Yang  <https://orcid.org/0000-0003-4411-7043>

### Supplemental Material

Supplemental material for this article is available online.

### References

Atkinson, J. J., & Senior, R. M. (2003). Matrix metalloproteinase-9 in lung remodeling. *American Journal of Respiratory Cell and*

*Molecular Biology*, 28(1), 12–24. <https://doi.org/10.1165/rcmb.2002-0166TR>

- Chen, Q., Jin, M., Yang, F., Zhu, J., Xiao, Q., & Zhang, L. (2013). Matrix metalloproteinases: Inflammatory regulators of cell behaviors in vascular formation and remodeling. *Mediators of Inflammation*, 2013, article ID 928315. <https://doi.org/10.1155/2013/928315>
- Chew, L. J., Pan, H., Yu, J., Tian, S., Huang, W. Q., Zhang, J. Y., Pang, S., & Li, L. Y. (2002). A novel secreted splice variant of vascular endothelial cell growth inhibitor. *The FASEB Journal*, 16(7), 742–744. <https://doi.org/10.1096/fj.01-0757fje>
- Christoffersson, G., Vågesjö, J., Vandooren, J., Lidén, M., Massena, S., Reinert, R., Brissova, M., Powers, A., Opdenakker, G., & Phillipson, M. (2012). VEGF-A recruits a proangiogenic MMP-9-delivering neutrophil subset that induces angiogenesis in transplanted hypoxic tissue. *Blood*, 120(23), 4653–4662. <https://doi.org/10.1182/blood-2012-04-421040>
- Duan, X., Wen, Z., Shen, H., Shen, M., & Chen, G. (2016). Intracerebral hemorrhage, oxidative stress, and antioxidant therapy, oxidative medicine and cellular longevity. *Oxidative Medicine and Cellular Longevity*, 2016, article ID 1203285. <https://doi.org/10.1155/2016/1203285>
- Gao, W., Zhao, Z., Yu, G., Zhou, Z., Zhou, Y., Hu, T., Jiang, R., & Zhang, J. (2015). VEG1 attenuates the inflammatory injury and disruption of blood–brain barrier partly by suppressing the TLR4/NF- $\kappa$ B signaling pathway in experimental traumatic brain injury. *Brain Research*, 1622 (5), 230–239. <https://doi.org/10.1016/j.brainres.2015.04.035>
- Gokhale, S., Caplan, L. R., & James, M. L. (2015). Sex differences in incidence, pathophysiology, and outcome of primary intracerebral hemorrhage. *Stroke*, 46(3), 886–892. <https://doi.org/10.1161/STROKEAHA.114.007682>
- Hansen, T. M., Moss, A., & Brindle, N. (2008). Vascular endothelial growth factor and angiopoietins in neurovascular regeneration and protection following stroke. *Current Neurovascular Research*, 5(4), 236–245. <https://doi.org/10.2174/156720208786413433>
- Kerber, M., Reiss, Y., Wickersheim, A., Jugold, M., Kiessling, F., Heil, M., Tchaikovski, V., Waltenberger, J., Shibuya, M., Plate, K. H., & Machein, M. R. (2008). Flt-1 signaling in macrophages promotes glioma growth in vivo. *Cancer Research*, 68(18), 7342–7351. <https://doi.org/10.1158/0008-5472.CAN-07-6241>
- Lapchak, P. A., Chapman, D. F., & Zivin, J. A. (2000). Metalloproteinase inhibition reduces thrombolytic (tissue plasminogen activator)-induced hemorrhage after thromboembolic stroke. *Stroke*, 31(12), 3034–3040. <https://doi.org/10.1161/01.STR.31.12.3034>
- Lee, S. J., Tsang, P. S., Diaz, T. M., Wei, B. Y., & Stetler-Stevenson, W. G. (2010). TIMP-2 modulates VEGFR-2 phosphorylation and enhances phosphodiesterase activity in endothelial cells. *Laboratory Investigation*, 90(3), 374–382. <https://doi.org/10.1038/labinvest.2009.136>
- Marini, S., Morotti, A., Ayres, A. M., Crawford, K., Kourkoulis, C. E., Lena, U. K., Gurol, E. M., Viswanathan, A., Goldstein, J. N., Greenberg, S. M., Biffi, A., Rosand, J., & Anderson, C. D. (2017). Sex differences in intracerebral hemorrhage expansion and mortality. *Journal of the Neurological Sciences*, 379, 112–116. <https://doi.org/10.1016/j.jns.2017.05.057>
- Nag, S., Takahashi, J. L., & Kilty, D. W. (1997). Role of vascular endothelial growth factor in blood–brain barrier breakdown and angiogenesis in brain trauma. *Journal of Neuropathology and*

- Experimental Neurology*, 56(8), 912–921. <https://doi.org/10.1097/00005072-199708000-00009>
- Pfefferkorn, T., & Rosenberg, G. A. (2003). Closure of the blood–brain barrier by matrix metalloproteinase inhibition reduces rtPA-mediated mortality in cerebral ischemia with delayed reperfusion. *Stroke*, 34(8), 2025–2030. <https://doi.org/10.1161/01.STR.0000083051.93319.28>
- Qi, J., Qin, T., Xu, L., Zhang, K., Yang, G.-L., Li, J., Xiao, H., Zhang, Z., & Li, L.-Y. (2013). TNFSF15 inhibits vasculogenesis by regulating relative levels of membrane-bound and soluble isoforms of VEGF receptor 1. *Proceedings of the National Academy of Sciences of the United States of America*, 110(34), 13863–13868. <https://doi.org/10.1073/pnas.1304529110>
- Qin, T., Xu, G., Qi, J., Yang, G.-L., Zhang, K., Liu, H., Xu, L., Xiang, R., Xiao, G., Cao, H., Wei, Y., Zhang, Q., & Li, L.-Y. (2015). Tumour necrosis factor superfamily member 15 (TNFSF15) facilitates lymphangiogenesis via up-regulation of VEGFR3 gene expression in lymphatic endothelial cells. *The Journal of Pathology*, 237(3), 307–318. <https://doi.org/10.1002/path.4577>
- Rempe, R. G., Hartz, A. M. S., & Bauer, B. (2016). Matrix metalloproteinases in the brain and blood–brain barrier: Versatile breakers and makers. *Journal of Cerebral Blood Flow & Metabolism*, 36(9), 1481–1507. <https://doi.org/10.1177/0271678X16655551>
- Rosenberg, G. A., & Navratil, M. (1997). Metalloproteinase inhibition blocks edema in intracerebral hemorrhage in the rat. *Neurology*, 48(4), 921–926. <https://doi.org/10.1212/WNL.48.4.921>
- Rundhaug, J. E. (2005). Matrix metalloproteinases and angiogenesis. *Journal of Cellular and Molecular Medicine*, 9(2), 267–285. <https://doi.org/10.1111/j.1582-4934.2005.tb00355.x>
- Schmued, L. C., & Hopkins, K. J. (2000). Fluoro-Jade B: A high affinity fluorescent marker for the localization of neuronal degeneration. *Brain Research*, 874(2), 123–130. [https://doi.org/10.1016/S0006-8993\(00\)02513-0](https://doi.org/10.1016/S0006-8993(00)02513-0)
- Seo, D.-W., Li, H., Guedez, L., Wingfield, P. T., Diaz, T., Salloum, R., Wei, B.-y., & Stetler-Stevenson, W. G. (2003). TIMP-2 mediated inhibition of angiogenesis. *Cell*, 114(2), 171–180. [https://doi.org/10.1016/S0092-8674\(03\)00551-8](https://doi.org/10.1016/S0092-8674(03)00551-8)
- Urday, S., Kimberly, W. T., Beslow, L. A., Vortmeyer, A. O., Selim, M. H., Rosand, J., Simard, J. M., & Sheth, K. N. (2015). Targeting secondary injury in intracerebral haemorrhage–perihematomal oedema. *Nature Reviews. Neurology*, 11(2), 111–122. <https://doi.org/10.1038/nrneurol.2014.264>
- Valable, S., Montaner, J., Bellail, A., Berezowski, V., Brillault, J., Cecchelli, R., Divoux, D., MacKenzie, E. T., Bernaudin, M., Roussel, S., & Petit, E. (2005). VEGF-induced BBB permeability is associated with an MMP-9 activity increase in cerebral ischemia: Both effects decreased by ANG-1. *Journal of Cerebral Blood Flow & Metabolism*, 25(11), 1491–1504. <https://doi.org/10.1038/sj.jcbfm.9600148>
- Wang, J., & Doré, S. (2007). Inflammation after intracerebral hemorrhage. *Journal of Cerebral Blood Flow & Metabolism*, 27(5), 894–908. <https://doi.org/10.1038/sj.jcbfm.9600403>
- Wang, J., Rogove, A. D., Tsirka, A. E., & Tsirka, S. E. (2003). Protective role of tuftsin fragment 1-3 in an animal model of intracerebral hemorrhage. *Annals of Neurology*, 54(5), 655–664. <https://doi.org/10.1002/ana.10750>
- Wang, J., & Tsirka, S. E. (2005). Neuroprotection by inhibition of matrix metalloproteinases in a mouse model of intracerebral haemorrhage. *Brain*, 128(7), 1622–1633. <https://doi.org/10.1093/brain/awh489>
- Wang, Y., Chen, J., Yang, L., Li, J., Wu, W., Huang, M., Lin, L., & Su, S. (2019). Tumor-contacted neutrophils promote metastasis by a CD90-TIMP-1 juxtacrine–paracrine loop. *Clinical Cancer Research*, 25(6), 1957–1969. <https://doi.org/10.1158/1078-0432.CCR-18-2544>
- Yang, G.-L., Han, Z., Xiong, J., Wang, S., Wei, H., Qin, T., Xiao, H., Liu, Y., Xu, L., Qi, J., Zhang, Z., Jiang, R., Zhang, J., & Li, L.-Y. (2019). Inhibition of intracranial hemangioma growth and hemorrhage by TNFSF15. *The FASEB Journal*, 33(9), 10505–10514. <https://doi.org/10.1096/fj.201802758RRR>
- Yang, G.-L., Zhao, Z., Qin, T., Wang, D., Chen, L., Xiang, R., Xi, Z., Jiang, R., Zhang, Z., Zhang, J., & Li, L.-Y. (2017). TNFSF15 inhibits VEGF-stimulated vascular hyperpermeability by inducing VEGFR2 dephosphorylation. *The FASEB Journal*, 31(5), 2001–2012. <https://doi.org/10.1096/fj.201600800R>
- Yu, J., Tian, S., Metheny-Barlow, L., Chew, L. J., Hayes, A. J., Pan, H., Yu, G. L., & Li, L. Y. (2001). Modulation of endothelial cell growth arrest and apoptosis by vascular endothelial growth inhibitor. *Circulation Research*, 89(12), 1161–1167. <https://doi.org/10.1161/hh2401.101909>
- Zhai, Y., Ni, J., Jiang, G. W., Lu, J., Xing, L., Lincoln, C., Carter, K. C., Janat, F., Kozak, D., Xu, S., Rojas, L., Aggarwal, B. B., Ruben, S., Li, L. Y., Gentz, R., & Yu, G. L. (1999). VEG1, a novel cytokine of the tumor necrosis factor family, is an angiogenesis inhibitor that suppresses the growth of colon carcinomas in vivo. *The FASEB Journal*, 13(1), 181–189. <https://doi.org/10.1096/fasebj.13.1.181>
- Zhu, H., Wang, Z., Yu, J., Yang, X., He, F., Liu, Z., Che, F., Chen, X., Ren, H., Hong, M., & Wang, J. (2019). Role and mechanisms of cytokines in the secondary brain injury after intracerebral hemorrhage. *Progress in Neurobiology*, 178, 101610. <https://doi.org/10.1016/j.pneurobio.2019.03.003>